Article

Solvothermally Synthesized Nickel-Doped Marigold-Like SnS$_2$ Microflowers for High-Performance Supercapacitor Electrode Materials

Ravindra Kumar, Ashish Kumar Keshari, Susanta Sinha Roy, Geetika Patel, and Gurupada Maity*

Read Online

ACCESS | Metrics & More | Article Recommendations

ABSTRACT: Two-dimensional transition-metal dichalcogenides (TMDs) have emerged as promising capacitive materials for supercapacitors owing to their layered structure, high specific capacity, and large surface area. Herein, Ni-doped SnS$_2$ microflowers were successfully synthesized via a facile one-step solvothermal approach. The obtained Ni-doped SnS$_2$ microflowers exhibited a high specific capacitances of 459.5 and 77.22 F g^{-1} at current densities of 2 and 10 A g^{-1}, respectively, in NaClO$_4$ electrolyte, which was found to be higher than that of SnS$_2$-based electrodes in various electrolytes such as KOH, KCl, Na$_2$SO$_4$, NaOH, and NaNO$_3$. Additionally, these microflowers demonstrate a good specific energy density of up to 51.69 Wh kg^{-1}, at a power density of 3204 Wkg^{-1}. Moreover, Ni-doped SnS$_2$ microflowers exhibit a capacity retention of 78.4% even after 5000 cycles. Better electrochemical performance of the prepared electrode may be attributed to some important factors, including the utilization of a highly ionic conductive and less viscous NaClO$_4$ electrolyte, incorporation of Ni as a dopant, and the marigold flower-like morphology of the Ni-doped SnS$_2$. Thus, Ni-doped SnS$_2$ is a promising electrode material in unconventional high-energy storage technologies.
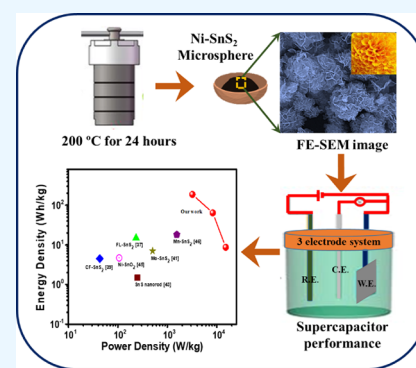
1. INTRODUCTION

Recently, the global development of industry, agriculture, and increasing consumption of fossil fuels have resulted in worsening energy crises and environmental pollution.[1,2] Therefore, it is urgent to develop cost-effective, environment friendly, cutting-edge devices and technologies. Supercapacitors, as green energy storage devices, have attracted enormous interest both in industry and academia owing to their distinctive attributes, including high power density, fast charge—discharge rate, long lifespan, excellent rate capability, reversibility, and more. However, their development and applications are mainly hampered due to their low energy as well as power density.[3−6] On the basis of the charge storage mechanism, supercapacitors may be sorted as electric double-layer capacitors (EDLCs) where the energy is mainly stored by ion adsorption/desorption at the electrode/electrolyte inter-face and pseudocapacitors where the energy is stored in the term of surface faradic reactions.[7,8] As is well-known, the electrochemical performance of supercapacitors highly relies on the intrinsic properties of critical electrode materials utilized in them.[4,9] From the material properties' perspective, it is essential to have high conductivity (electronic/ionic), easy ion transportation, high porous, and a high surface area.[10]

Various carbonaceous materials such as graphene, activated carbons, and carbon nanotubes (CNTs) have been predominantly utilized as electrode precursors in supercapacitors owing to their unmatched physiochemical properties such as superior electronic conductivity, low cost, low density, regulated pore structure, high corrosion resistance, huge specific surface area, and electrochemical stability.[11−13] However, their practical applications have been restricted due to their many unconventional characteristics, including low energy density (<10 Wh/kg) due to sluggish mass diffusion, limited charge accumulation, low capacitance, and complex synthesis procedures.[8,11,14,15] Henceforth, it is imperative to develop a viable alternative of EDLCs as an electrode for supercapacitor applications. Pseudocapacitive materials excel in this role, owing to their high energy density and theoretical specific capacities, which can be attributed to their faradaic redox reactions.[16,17] Therefore, the performance of the SCs can be improved by selecting and designing advanced electrode materials.
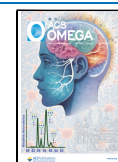
Transition metal dichalcogenides (TMDs) are grouped as a class of pseudocapacitive materials and are extensively studied for energy storage purposes due to their high capacity and high

power density, which can be attributed to their high surface areas, layered structure, and electronic conductivities. TMDs exhibit scientific significance because they possess unique structures, good physiochemical properties, reversible redox reactions, low toxicity, low cost, and natural abundance.[18−20] Among them, tin disulfide (SnS_2) has emerged as a promising electrode material owing to its salient features, such as CdI_2-type hexagonal layered structure, similar to that predominantly used graphite, a larger interlayer spacing of 5.9 A^0, high chemical stability, environment-friendliness, and cost-effectiveness.[21,22] These devices have been successful to find their applications in the range of devices, including photocatalysis,[23] photoelectrocatalysis,[24] dye-sensitized solar cells,[25] biosensors,[26] lithium-ion battery,[27] sodium-ion battery,[28] and supercapacitors.[29] However, their practical application is limited due to their inadequate conductivity which leads to poor electrochemical performance. With the aim of improving the electrochemical performance of SnS_2, many effective strategies have implemented, such as doping of metal/nonmetal ions, that alter the band structure of SnS_2 to improve the electrochemical performances. These modifications are responsible for providing new possibilities and improved performance in the desired applications.[30−32]

In previous research studies, metal-doped SnS_2 (e.g., Cu, Mn, Ni, Co, Mo, Pt, Ag, Zn, etc.) has been used for various applications, such as lithium-ion batteries, sodium-ion batteries, and electrocatalytic hydrogen evolution reactions fields.[33−36] Among them, Ni can be used as a crucial dopant because of its merits, such as less expensive, low toxicity, and high chemical stability. More importantly, Ni^{2+} has an ionic radius similar to that of Sn^{4+} which helps Ni to be easily doped into the SnS_2 lattice.[34] Because of the aforementioned advantages, SnS_2 nanomaterials doped with Ni are highly appreciated. Recently, many studies have demonstrated improved electrochemical performance of nanomaterials based on SnS_2 for supercapacitor applications. For example, Parveen et al. used a one-step solvothermal method to prepare SnS_2 nanostructures with different morphologies, employing with KOH electrolyte solution. They found that flower-like SnS_2 exhibits better electrochemical performance with a high capacity of ~431.82 F g^{-1}, an energy density of 14.9 Wh kg^{-1}, and a power density of 233 W kg^{-1} at a current density of 1 A g^{-1} compared with other morphologies such as sheet-like SnS_2.[37] Wang et al. synthesized a 3D flower-like SnS_2/MoS_2 heterostructure via a hydrothermal process and exhibited the specific capacitance of 105.7 F g^{-1} at a current density of 2.35 A g^1 with the capacity retention of 90.4% up to 1000 cycles in a KCl electrolyte solution.[38] Also, Mishra et al. synthesized flower-like SnS_2 via a one-step solvothermal approach and reported a specific capacitance of 215 F g^{-1}, energy density of 4.52 Wh kg^{-1}, and power density of 43.10 W kg^{-1}, at the current density of 0.38 A g^{-1} with the capacity retention of 66% after 1000 cycles.[39] Ansari et al. synthesized 3D flower-like $SnS_2@g-C_3N_4$ sheets using a facile solvothermal approach and reported a specific capacitance of 178 F g^{-1}, energy density of 4.7 Wh kg^{-1}, power density of 200 W kg^{-1} at the current density of 1A g^{-1}, and maintained capacity retention of 84% up to 1500 cycles, in KOH electrolyte solution.[40] Also, Ma et al. synthesized Mo-doped SnS_2 via a hydrothermal process and reported a specific capacitance of 213 F g^{-1}, energy density of 7 Wh kg^{-1}, and power density of 504 W kg^{-1} at the current density of 1 A g^{-1} with capacity retention of 89% up to 1000 cycles in KOH electrolyte solution.[41] In their research work,

Asen et al. synthesized SnS_2/SnO_2 nanohetrostructure via a solvothermal approach and reported a specific capacitance of 149 F g^{-1} at the current density of 2 A g^{-1} and also exhibited capacity retention of 92% up to 3000 cycles in Na_2SO_4 electrolyte solution.[42] In another research, Chauhan et al. synthesized SnS nanorods via solvothermal route showed a specific capacitance of 70 F g^{-1} at the current density of 0.5 $mAcm^{-2}$ up to 500 cycles in Na_2SO_4 electrolyte solution.[43] Sajad et al. synthesized SnS_2 nanorods via adopting a facile hydrothermal method and exhibited a specific capacitance of 162 F g^{-1} at a current density of 3 A g^{-1} with the cycling stability of 93% after 4000 cycles.[44] Meng et al. synthesized Ni-doped SnO_2 nanoflower via adopting a simple hydrothermal process and showed a specific capacitance of 410 mF cm^{-2} at the scan rate of 1 $mAcm^{-2}$ and maintained a cycling stability of 93.6% up to 2500 cycles in NaOH electrolyte solution.[45] More recently, Chu et al. synthesized Ni, Co-doped SnS_2−graphene aerogel (Ni-SnS_2-GA, Co-SnS_2-GA, and Mn-SnS_2-GA) via a solvothermal method. In supercapacitor performance Ni-SnS_2-GA, and Co-SnS_2-GA showed specific capacitance with values of 154 and 207 F g^{-1}, the energy density of 18.1 Wh kg^{-1}, and power density of 1550 W kg^{-1} for Ni-SnS_2-GA, respectively, at the current density of 1 A g^{-1} and maintained a cycling stability of 65%, and 93.66% after 2000 cycles in 6 M KOH electrolyte.[46] Previous studies have shown that various SnS_2-based electrodes paired with different electrolytes, such as KOH, KCl, Na_2SO_4, NaOH, and $NaNO_3$, have been employed for supercapacitor applications. Nevertheless, these pairs exhibit inferior electrochemical performance characterized by lower energy density and power density. Hence, it is essential to use SnS_2-based electrodes with appropriate electrolytes to improve the electrochemical performance of supercapacitors.

Presently, Water-in-Salt Electrolyte (WiSE), such as $NaClO_4$, has received great interest owing to expended electrochemical stability window (up to 6 V), decent ionic conductivity, lower viscosity (5.0 mm^2 s^{-1}), low vapor pressure, low cost, and nonflammability high thermal stability. These properties directly contribute to enhance the energy density of energy storage devices. However, to the best our knowledge, no research study has employed a Ni-doped SnS_2 electrode along with a $NaClO_4$ electrolyte for supercapacitor applications.[47]

In the present study, Ni-doped marigold-like SnS_2 microflower were fabricated via a one-step solvothermal process, and used as active electrode materials in conjunction with $NaClO_4$ for supercapacitor applications. The samples were characterized by several characterization techniques, including X-ray diffraction (XRD), Raman measurements, X-ray photoelectron spectroscopy (XPS), field emission scanning electron microscope (FESEM), and Transmission Electron Microscopy (TEM). The electrochemical performances of the as-synthesized Ni-doped marigold-like SnS_2 microflower electrode were examined through electrochemical tests, such as cyclic voltammetry (CV) curves, galvanostatic charge−discharge (GCD) curves, and electrochemical spectroscopy (EIS). The doping of Ni and utilization of $NaClO_4$ as an electrolyte are effective strategies to enhance the electrochemical performances of SnS_2-based supercapacitor.

2. EXPERIMENTAL SECTION

2.1. Chemical and Materials. Tin(II) chloride dihydrate ($SnCl_2 \cdot 2H_2O$), nickle (II) chloride hexahydrate ($NiCl_2 \cdot 6H_2O$), and thioacetamide (C_2H_5NS) were purchased from

Sigma-Aldrich. All materials were used without further purification.

2.2. Preparation of Ni-Doped Marigold-Like SnS₂ Microflower and Pure SnS₂. SnS₂ and Ni-doped SnS₂ powders were synthesized through a facile one-step solvo-thermal method. In this typical procedure, 0.3506 g of SnCl4·5H₂O is initially dissolved in a 30 mL mixture of ethanol and isopropanol. Following stirring for 10 min, 0.036 g of NiCl₂·6H₂O was added to the above solution. After another stirring for 10 min, 0.1503 g of thioacetamide was dissolved in the above solution.

Next, the mixture was stirred for another 10 min to obtain a homogeneous solution. Subsequently, this homogeneous solution was transferred into an autoclave and reacted at 200 °C for 24 h. After allowing the reactor to cool down naturally to room temperature, the samples were washed several times with deionized water and absolute ethanol. Finally, the samples were dried in an oven at 80 °C overnight. According to the Ni-to-SnS₂ mass ratio $((x \text{ g}/0.1827 \text{ g}) \times 100\% = 10\%)$, the corresponding samples are referred to as 10% Ni-SnS₂. For comparison, pure SnS₂ was synthesized following the procedure with using NiCl₂·6H₂O. A schematic diagram of the Ni-SnS₂ synthesis process using the one-step solvothermal method is shown in Figure 1.
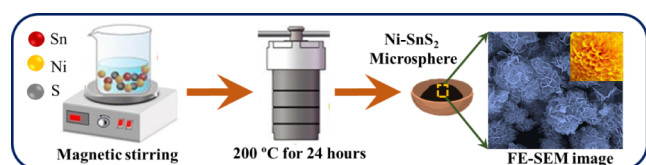

Figure 1. Schematic diagram of the Ni-SnS₂ synthesis process using the one-step solvothermal method.

2.3. Preparation of Electrodes. The procedure for preparing the working electrodes of the obtained samples is summarized below. Active material, carbon black, and polyvinylidene fluoride (PVDF) were mixed in a weight ratio of 7:2:1, and N-methyl-2-pyrrlodone (NMP) was dropped into the mixture to obtain a slurry. The slurry was evenly speared onto a carbon cloth (CC) and then dried at about 120 °C in vacuum overnight. The mass loading of the active materials on CC was calculated to be 3.5 mg/cm².

2.4. Characterization Methods. The morphologies and structures of the as-synthesized Ni-doped SnS₂ microflowers were analyzed by field-emission scanning electron microscopy (FESEM) using FESEM JEOL JSM 7600 PLUS, Tokyo, Japan. The crystal structure and elemental composition of the prepared samples were confirmed by X-ray diffraction (XRD) in coupled θ-2θ diffraction (Bruker D8 discover, Karlsruhe, Germany) using Cu−Kα radiation. Also, trans-mission electron microscopy (TEM) measurements were utilized for further structural confirmation. Raman spectra were obtained using a Renishaw microscope with He−Ne laser operating at a wavelength of 514 nm as the excitation source. In order to determine the elemental composition of the samples, energy-dispersive X-ray (EDX) measurements were performed. For further analysis, X-ray photoelectron spectros-copy (XPS) measurements were carried out.

2.5. Electrochemical Measurements. The electrochem-ical capacitive performance of the prepared samples was measured using an Autolab potentiostat/galvanostat 302N instrument (Metrohm B.V. Utrecht, the Netherlands) controlled by Nova (version 1.10) software uisng a three-electrode system. These performances were tested in a 1 M NaClO₄ aqueous electrolyte solution. In order to prepare a 1 M solution of NaClO₄ electrolyte, we have dissolved 4.89 g of NaClO₄ in 40 mL of distilled water. Platinum (Pt) rod and silver−silver chloride (Ag/AgCl) were used as the counter
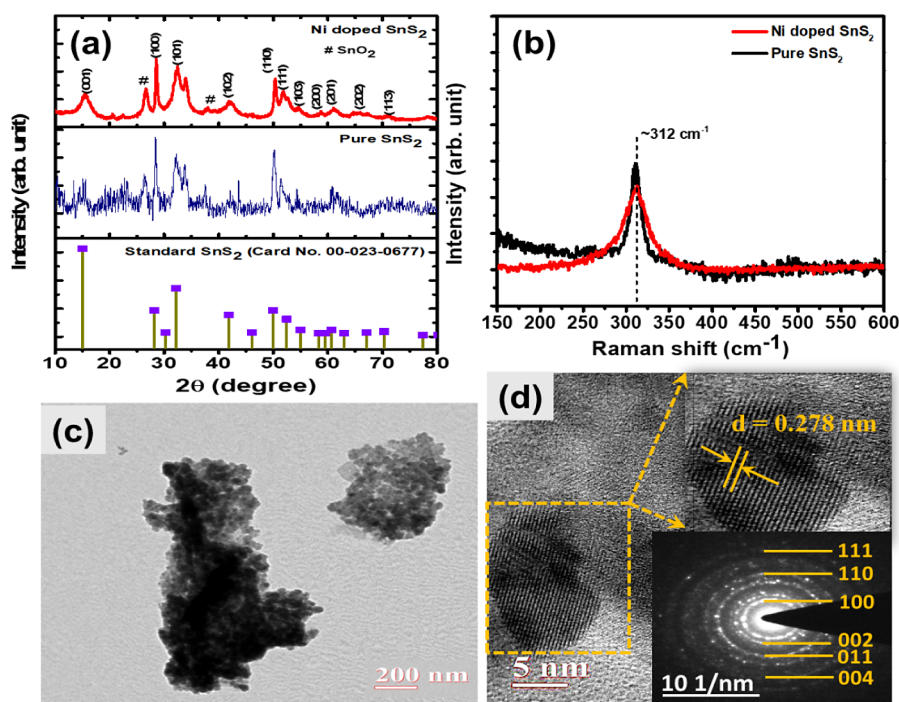

Figure 2. (a) XRD pattern, (b) Raman spectra, (c) TEM image, (d) HRTEM image of Ni-SnS₂ microflowers (SAED pattern shown in inset).
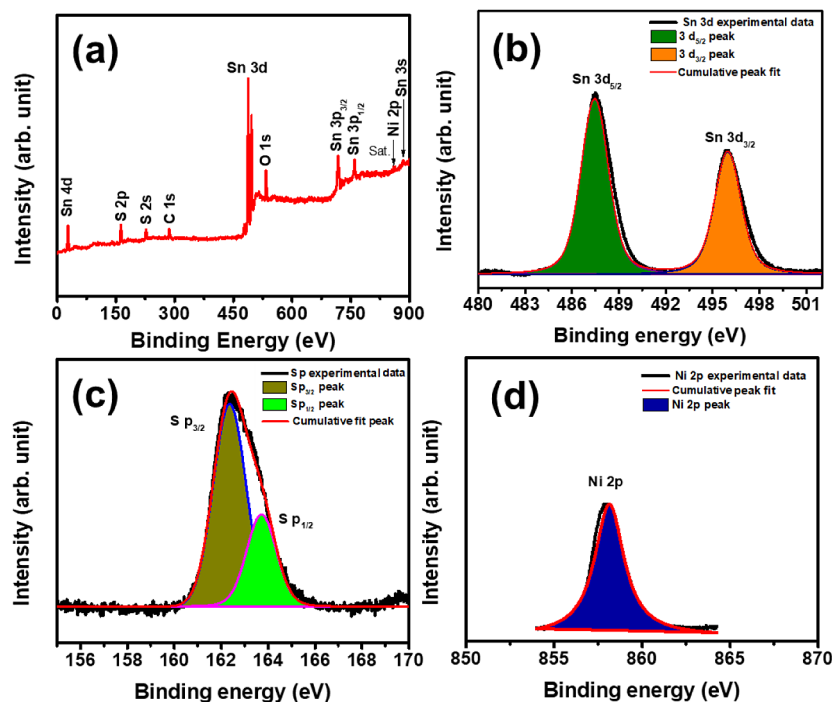
Figure 3. (a) Full X-ray photoelectron spectra of Ni-SnS₂. (b) High-resolution X-ray photoelectron spectra of Sn 3d. (c) High-resolution X-ray photoelectron spectra of S 2p. (d) High-resolution X-ray photoelectron spectra of Ni 2p.
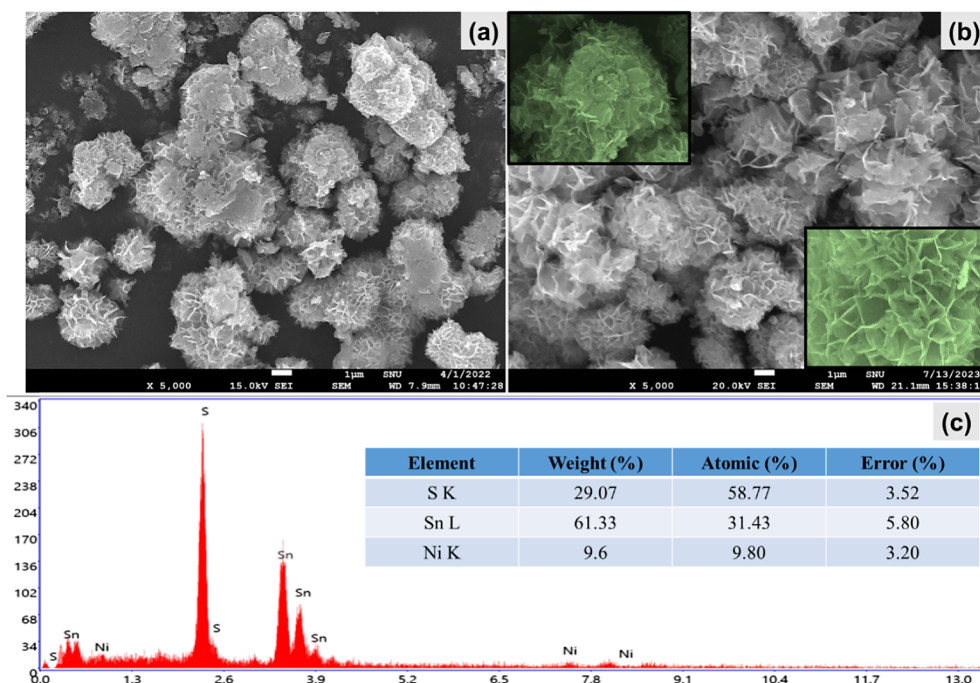

Figure 4. SEM images of (a) SnS₂ and (b) Ni-SnS₂. (c) EDX spectra of Ni-SnS₂.

electrode and reference electrode, respectively. The Ni-doped SnS₂ microflower working electrode was prepared directly as described in the previous section. Cyclic voltammetry (CV) measurements were recorded within the potential window of +0.9 to −0.2 V (vs Ag/AgCl) at a sweep rate of 10−50 mV s⁻¹. Galvanostatic charge−discharge (GCD) performancse were recorded within the potential range of 0.0 to −1.0 V (vs Ag/AgCl) within the current range of 1 to 10 A g⁻¹.

3. RESULT AND DISCUSSION

3.1. Structural Characterizations. The XRD patterns of the as-prepared powder are shown in Figure 2a. Most of the distinguishable XRD peaks of the obtained sample were well indexed with the standard card (PDF#23−0677) and are consistent with previous reports. These XRD peaks can be assigned to the hexagonal SnS₂ having the same crystalline structure.[35,46,48] The diffraction peaks were obtained at 15.15°, 28.47°, 32.32°, 42.05°, and 50.18°, respectively, which
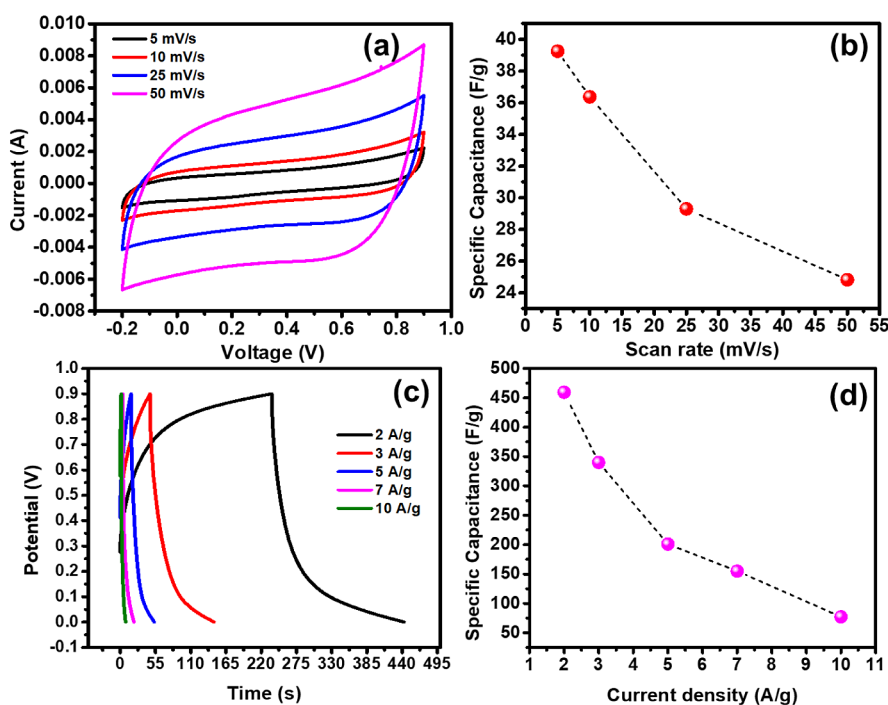
Figure 5. (a) CV curves at various scan rates; (b) specific capacitance as a function of scan rates; (c) GCD curves at various current densities; and (d) specific capacitance at different current densities.

correspond to the (001), (100) (101), (110), and (111) planes of SnS_2. Additionally, the two diffraction peaks at 26.7° and 38.0° indicate the impurity phase of SnO_2 which is due to the oxidation of the prepared samples in the atmosphere.

The structural quality of the $Ni-SnS_2$ microflower samples was also further characterized by Raman spectroscopy using the laser with a wavelength of 514 nm as the excitation source attained at room temperature. Figure 2b clearly shows the Raman spectra collected from pure SnS_2 and $Ni-SnS_2$ microflower, from which it was observed that there was only a single Raman peak centered at 312 cm^{-1} that can be ascribed to the A_{1g} mode of SnS_2.[49] Apparently, from the obtained Raman spectra, it can be clearly seen that there were no additional peaks indicating the absence of other Raman modes of SnS_2. Infact, the Raman characterization of the as-synthesized $Ni-SnS_2$ microflower more clearly shows the stretching mode of S−Sn−S bonds which is also consistent with previous studies.[50] These results confirm the formation of the SnS_2 phase. It should be noted here that there is a decrement in peak intensity and an increment in broadening of the Raman spectra of Ni-doped sample compared to the pure one. These results suggest that the doped sample exhibits a more amorphous nature than the pure sample. Further, structural confirmation of the as-prepared sample was done by the TEM measurements. Figure 2c shows the TEM image of the $Ni-SnS_2$ microflower. It is clearly observed that the morphology looks like a marigold-like microflower. The high-resolution TEM (HRTEM) of this sample is shown in Figure 2d. As can be seen from the figure, the d spacing was found to be 0.278 nm, which corresponds to the SnS_2 (101) diffraction plane. The SAED pattern of the sample is shown in the inset, and it is consistent with the XRD results. The chemical compositions and valence states of $Ni-SnS_2$ microspheres sample were examined via XPS, as shown in Figure 3a. No other impurity signals were observed except for Sn, S, C, O,

and Ni in $Ni-SnS_2$, indicating that Ni cation was successfully introduced into SnS_2. Additionally, in Figure 3a, the core-level XPS spectra of Ni 2p and Sn 3s are also observed (marked as "Sat."). Figure 3b shows the high-resolution survey spectrum of Sn 3d, showing two clear peaks located at 495.3 and 486.6 eV corresponding to Sn $3d_{3/2}$ and Sn $3d_{5/2}$, respectively, attributed to tetravalent Sn^{4+} without any apparent peaks corresponding to divalent Sn^{2+}.[50] The S 2p spectrum shown in Figure 3c shows two peaks located at 162.6 and 161.5 eV, which can be ascribed to S $2p_{1/2}$ and S $2p_{3/2}$, respectively, which can be ascribed to divalent S^{2-}.[50,51] Figure 3d shows a peak centered at 854.8 eV corresponding to which is ascribed to Ni^{2+}.[52]

The surface morphologies and structures of the as-synthesized pure and Ni-doped SnS_2 samples were confirmed by FESEM, as shown Figure 4a,b. From high-magnification FESEM of pure SnS_2, as seen in Figure 4a, a microflower-like structure was observed. Figure 4b clearly shows the growth of $Ni-SnS_2$ microflower (see in inset Figure 4b).

Figure 4c demonstrates the EDX spectra of the $Ni-SnS_2$ microflowers. It can be observed that the obtained sample contains the elements Sn, S, and Ni. Additionally, the atomic percentage compositions of the present elements Sn, S, and Ni are also shown in Figure 4C that indicates the uniform distribution of all elements in the sample.

3.2. Electrochemical Investigations. The electrochemical performance of the $Ni-SnS_2$ microflowers are evaluated in a three-electrode system using 1 M sodium perchlorate $(NaClO_4)$ as an electrolyte solution and $Ni-SnS_2$ as a working electrode. Figure 5 shows the cyclic voltammograms (CVs) of the prepared electrode at rates 5 mV s^{-1}, 10 mV s^{-1}, 25 mV s^{-1}, and, 50 mV s^{-1} in the potential range of −0.2 to +0.9 V. It can be observed from CV curves that the area of $Ni-SnS_2$ is found to be increased with the increasing scan rate.

The specific capacitance (C_s) values of the electrode were calculated utilizing the following formula:
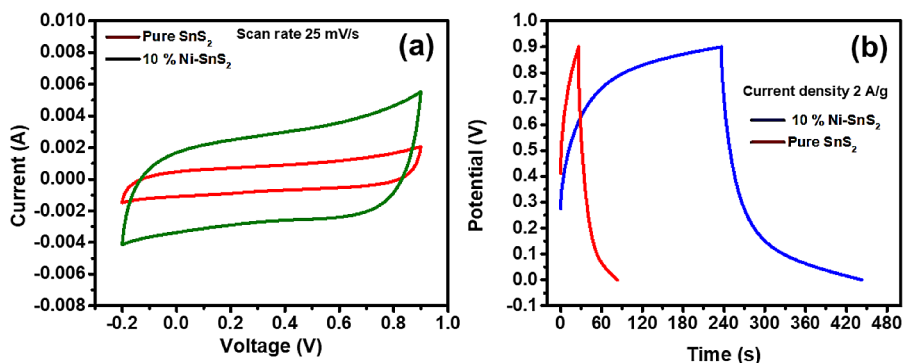
Figure 6. (a) CV curves of SnS$_2$ and Ni-SnS$_2$ at 25 mV s^{-1} (b) GCD curves of SnS$_2$ and Ni-SnS$_2$ at 2 A g^{-1}.

$$C_s = \frac{A}{2mk\Delta V} \qquad (1)$$

where A, m, k, and ΔV are the areas, masses of the active electrode materials, sweeping rates, and potential windows, respectively. The specific capacitance values of 39.25, 36.37, 29.30, and 24.82 F g^{-1} were obtained for Ni-SnS$_2$ microspheres at scan rates of 5 mV s^{-1}, 10 mV s^{-1}, 25 mV s^{-1}, and 50 mV s^{-1}, respectively. Figure 5b shows the specific capacitance at different current densities. The galvanostaic charge−discharge (GCD) curves for the fabricated electrodes of the Ni-SnS$_2$ microspheres were recorded at different current densities of 2, 3, 5, 7, and 10 A g^{-1} within the potential range of 0.0 to 0.9 V (vs Ag/AgCl), as shown in Figure 5c. As can be observed from the GCD curves, there is a significant deviation from the triangular shapes, indicating that the prepared material exhibits pseudocapacitive characteristics, which is in good agreement with the CVs result.

The specific capacitance values from the GCD curves were calculated by using the following equation:

$$C_s = \frac{I\Delta t}{m\Delta V} \qquad (2)$$

where C_s is the specific capacitance (F g^{-1}), I is the current density (A g^{-1}), Δt is the discharging time (s), ΔV is the potential window, and m is the loaded mass of the active material.

The specific capacitances of the prepared electrode were calculated by using eq 2 are 459.5, 340.0, 201.2, 155.0, 77.22 F g^{-1} for the nanostructures at the current density of 2, 3, 5, 7, and 10 Ag^{1-}, respectively. The prepared electrode from the Ni-SnS$_2$ microflowers exhibits the higher specific capacitance, which may be attributed to the doping of Ni metal that improves the active sites that are helpful to improve the electrochemical performances of supercapacitors. Moreover, as well-known, the morphology also influences the electrochemical performance of the prepared electrode. Figure 5d shows the specific capacitance at different current densities.

For comparison, the electrochemical performances between pure SnS$_2$ and Ni-SnS$_2$, CV tests were conducted at the scan rate of 25 mV s^{-1} with potentials ranging from −0.2 to +0.9 V, as shown in Figure 6a. Figure 6a shows that the area of Ni-SnS$_2$ is larger than that of pure SnS$_2$, indicating that the doped Ni-SnS$_2$ has a higher specific capacitance compared to pure SnS$_2$. In the same text, GCD tests were also conducted at the current density of 2 A g^{-1} with potential ranging from −0.1 to 0.9 V, as depicted in the Figure 6b. Similarly, it can be seen that the discharging time of Ni-SnS$_2$ is longer than that of pure SnS$_2$,

further indicating that the doped Ni-SnS$_2$ has a larger specific capacitance compared to pure SnS$_2$, in good agreement with the CV results. The marigold flower-like Ni-SnS$_2$ microflower enhances the effective reactions between the electrolyte ions and active electrode materials, attributed to the enhancement of the active sites due to Ni doping in the SnS$_2$ crystal. This leads to a positive impact and improves the capacitive performance of the as-prepared electrode compared to pure SnS$_2$.

To understand the capacitive behavior of the prepared samples, in-depth electrochemical impedance spectroscopy (EIS) tests were conducted, and the Nyquist plots were obtained, as shown in Figure 7. From the Nyquist plots, we can
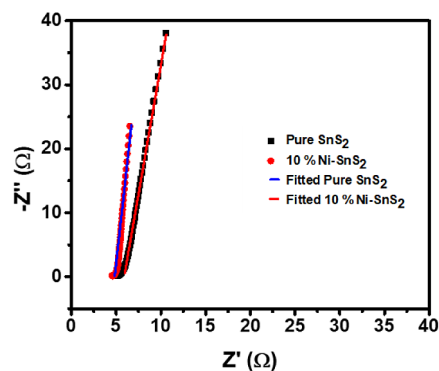

Figure 7. Nyquist plots of the SnS$_2$ and Ni-SnS$_2$ sample.

see that there was a nearly vertical straight line in the low-frequency range, which indicates better capacitive behavior and excellent conductivity of the samples. Moreover, from the obtained data, it can be seen that pure SnS$_2$ exhibits the higher interface impedance compared to Ni-SnS$_2$, for which Ni-SnS$_2$ exhibits better conductivity. The straight line shows an excellent capacitive behavior with little resistant component inclusions, suggesting that the highly conductive Ni-SnS2 electrode material is the source of low resistance to ionic diffusion.[39,41,46] This can be ascribed to doping of Ni ions, which resulted in crystal defects, and effectively improved the conductivity of the pure SnS$_2$.

Table 1 shows a comparison between the specific capacitances of previously reported various SnS$_2$-based materials. Various nanostructures were synthesized via different chemical routes, such as the hydrothermal method and solvothermal methods. The present work demonstrates the one-step solvothermal process for preparing Ni-SnS$_2$ microflower. The solvothermal approach has been widely adopted

Table 1. A Comparison among Specific Capacitances of Various SnS₂-Based Materials for Supercapacitor Energy Storage

materials	specific capacitance	current density or scan rate	electrolyte	references
SnS$_2$-g -C$_3$N$_4$	178 F g^{-1}	1 A g^{-1}	3.5 KOH	40
Mo-doped SnS$_2$	213 F g^{-1}	1 A g^{-1}	3.45 KOH	41
Ni/SnS$_2$ nanoflower	410 mF cm^{-2}	1 mA cm^{-2}	1 M NaOH	45
Ni-MnO$_2$	252.6 F g^{-1}	5 mV s^{-1}	NaNO$_3$	53
SnS$_2$ nanostructures	431 F g^{-1}	1 A g^{-1}	2 M KOH	37
SnS nanorods	70 F g^{-1}	1 mA cm^{-2}	1 M Na$_2$SO$_4$	43
SnS$_2$/MoS$_2$	105 F g^{-1}	2.3 A g^{-1}	1 M KCl	38
SnS$_2$ flower-like	215 F g^{-1}	0.38 A g^{-1}	1 M KCl	39
Ni-SnS$_2$-graphene aerogel	112 F g^{-1}	1 A g^{-1}	6 M KOH	46
Co-SnS$_2$-graphene aerogel	175 F g^{-1}	1 A g^{-1}	6 M KOH	46
Mo-SnS$_2$-graphene aerogel	323 F g^{-1}	1 A g^{-1}	6 M KOH	46
SnS$_2$–SnO$_2$ nanostructure	149 F g^{-1}	2 A g^{-1}	0.5 Na$_2$SO$_4$	42
Ni/ SnS$_2$microflower	459.5 F g^{-1}	2A g^{-1}	1 M NaClO$_4$	this work

because of its high efficiency, low processing time, and ease of handling. In the present work, one can clearly observe from the Table 1 that Ni-SnS$_2$ microflower exhibits better capacitive performance compared to the pure SnS$_2$. Therefore, the prepared Ni-SnS$_2$ microstructures can be utilized as active materials with comparatively good capacitive behavior for supercapacitor storage applications. In the present work, the high capacitance of Ni-SnS$_2$ was found as compared to previous reports, which might be due to three main factors: (i) the use of a water-in-salt electrolyte (WiSE), such as NaClO$_4$, possessing high ionic conductivity and lower viscosity;[47] (ii) doping of Ni, introducing various oxidation sates; and (iii) highly regular-shaped marigold-like structure.

capacitive retention was studied by performing cycle stability at the current density of 2 A g^{-1} and the retention was observed to be 78.4% up to 5000 cycles, as shown in Figure 8a.

The GCD curves were used to calculate the energy density (E) in Wh kg^{-1} and power density (P) in W kg^{-1} by the

following equations, and thus, they were plotted as shown in Figure 8b.

$$E = \frac{C_s (\Delta V)^2}{7.6} \tag{3}$$

$$P = \frac{E}{\Delta t} \tag{4}$$

where C_S is the specific capacitance of the suercapacitor (V), ΔV is the potential window of the supercapacitor (V), and Δt is the discharge time (s).

Figure 8b presents the Ragone plot, which compares the energy vs power densities of our Ni-SnS$_2$ microflowers with other reports. From Figure 8b, one can easily observe that previously reported, SnS$_2$-based electrodes with different electrolytes (KOH, KCl, Na$_2$SO$_4$, NaOH, and NaNO$_3$) exhibited lower energy and power densities. Furthermore, from Figure 8b, it can be seen that the energy density (maximum 51.69 Wh kg^{-1} at 2 A g^{-1}, also power density 3204 W kg^{-1}) decreases as the power density increases, but there is 78.4% retention even at 15 220 W kg^{-1} which indicates that Ni-SnS$_2$ is capable of showing excellent rate performance. It is worth noting here that the energy and power density of our samples shows higher than those of previously reported SnS$_2$-based materials. Moreover, high power density can be reached for practical applications without losing remarkable energy capacitance.

4. CONCLUSIONS

In summary, Ni-doped SnS$_2$ microflowers were successfully synthesized using a one-step solvothermal approach and exhibited better electrochemical performance compared to SnS$_2$. Moreover, the CC substrate with high mechanical strength to maintain the integrity of the Ni-doped SnS$_2$ microflower electrode during electrochemical testing. The prepared Ni-doped SnS$_2$ exhibited better electrochemical performance than SnS$_2$. The as-prepared Ni-doped SnS$_2$ electrode displayed a high specific capacitance of 459.5 F g^{-1} at a current density of 2 A g^{-1}, in the three-electrode systems and maintained the capacity retention of 78.4% after 5000 cycles. The high capacitance of Ni-SnS$_2$ mainly resulted from three main factors: (i) the use of a water-in-salt electrolyte (WiSE), NaClO$_4$, with high ionic conductivity and lower viscosity; (ii) doping with Ni, which exhibits various oxidation sates; (iii) the presence of a marigold-like morphology. Such better capacitive behaviors imply that the SnS$_2$ microflower-
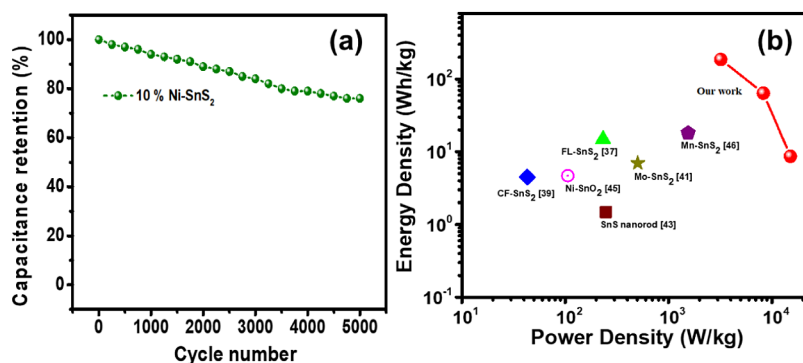

Figure 8. (a) Cyclic stability results. (b) Energy density and power density of the electrode at different charge/discharge rates and comparison with previous reports.

like, are promising active electrode materials for practical applications in various energy storage devices.

ASSOCIATED CONTENT

Data Availability Statement

The data that support the findings of this study are original and will available from the corresponding author upon reasonable request. The supporting data from other author are not included due to ethical and privacy restrictions to protect participant confidentiality and adhere to informed consent agreements.

AUTHOR INFORMATION

Corresponding Author

Gurupada Maity − *Department of Physics, Shiv Nadar University, Greater Noida 201314, India; Department of Physics, School of Basic and Applied Science, Galgotias University, Greater Noida 203201, India;* Present Address: R.K. and G.M. contributed equally to this work; orcid.org/0000-0003-0229-3014;
Email: gurupada.phy@gmail.com

Authors

Ravindra Kumar − *Department of Applied Physics, Gautam Buddha University, Greater Noida 210312, India;* Present Address: R.K. and G.M. contributed equally to this work

Ashish Kumar Keshari − *Department of Applied Physics, Gautam Buddha University, Greater Noida 210312, India;* orcid.org/0000-0003-2537-6605

Susanta Sinha Roy − *Department of Physics, Shiv Nadar University, Greater Noida 201314, India*

Geetika Patel − *Department of Chemistry, Shiv Nadar University, Greater Noida 201314, India*

Complete contact information is available at:
https://pubs.acs.org/10.1021/acsomega.4c03452

Notes

The authors declare no competing financial interest.

ACKNOWLEDGMENTS

REFERENCES

(1) Wang, T.; Chen, S.; Pang, H.; Xue, H.; Yu, Y. MoS$_2$ -Based Nanocomposites for Electrochemical Energy Storage. *Adv. Sci.* **2017**, *4* (2), 1600289.

(2) Yadlapalli, R. T.; Alla, R. R.; Kandipati, R.; Kotapati, A. Super capacitors for energy s- torage: Progress, applications and challenges. *J. Energy Storage* **2022**, *49*, 1600289.

(3) Zhang, J.; Gu, M.; Chen, X. Supercapacitors for renewable energy applications: A revie- w. *Micro- Nano Eng.* **2023**, *21*, 100229.

(4) Yu, J.; Fu, N.; Zhao, J.; Liu, R.; Li, F.; Du, Y.; Yang, Z. 2019. High specific capacitance electrode material for supercapacitors based on resin-derived nitrogen-doped porous carbon. *ACS Omega* **2019**, *4*, 15904−15911.

(5) Miao, L.; Qian, X.; Zhu, D.; Chen, T.; Ping, G.; Lv, Y.; Xiong, W.; Liu, Y.; Gan, L.; Liu, M. From interpenetrating polymer networks to hierarchical porous carbons for advanc- ed supercapacitor electrodes. *Chin. Chem. Lett.* **2019**, *30*, 1445−1449.

(6) Gao, G.; Lu, S.; Xiang, Y.; Dong, B.; Yan, W.; Ding, S. Free-standing ultrathin Co- Mn$_2$O$_4$ nanosheets anchored on reduced graphene oxide for high-performance supercapaci- tors. *Dalton Trans.* **2015**, *44*, 4418737−4418742.

(7) Choudhary, N.; Li, C.; Chung, H. S.; Moore, J.; Thomas, J.; Jung, Y. High-performance one-body core/shell nanowire super-capacitor enabled by conformal growth of capacitive 2D WS$_2$ layers. *ACS Nano* **2016**, *10*, 10726−10735.

(8) Karimi, Z.; Moon, J.; Malzahn, J.; Eddings, E.; Warren, R. Ultra-low cost supercapacitors from coal char: effect of electrolyte on double layer capacitance. *Energy Adv.* **2023**, *2*, 1036−1044.

(9) Wang, Z.; Xu, Z.; Huang, H.; Chu, X.; Xie, Y.; Xiong, D.; Yan, C.; Zhao, H.; Zhang, H.; Yang, W. Unraveling and regulating self-discharge behavior of Ti$_3$C$_2$Tx MXene-based supercapacitors. *ACS Nano* **2020**, *14*, 144916−144924.

(10) Chen, T.; Dai, L. Carbon nanomaterials for high-performance supercapacitors. *Mater. Today* **2013**, *16* (7−8), 272−280.

(11) Yang, B.; Zhang, W.; Zheng, W. Unlocking the full energy densities of carbon based supercapacitors. *Mater. Res. Lett.* **2023**, *11*, 517−546.

(12) Jayaseelan, S. S.; Radhakrishnan, S.; Saravanakumar, B.; Seo, M. K.; Khil, M. S.; Kim, H. Y.; Kim, B. S. Mesoporous 3D NiCo$_2$O$_4$/ MWCNT nanocomposite aerogels prepred by a supercritical CO$_2$ drying method for high performance hybrid supercapacitor electrodes. *Colloids Surf. A* **2018**, *538*, 451−459.

(13) Zheng, S.; Li, Q.; Xue, H.; Pang, H.; Xu, Q. A highly alkaline-stable metal oxide@ m- etal-organic framework composite for high-performance electrochemical energy storage. *Natl. Sci. Rev.* **2020**, *7*, 305−314.

(14) Borenstein, A.; Hanna, O.; Attias, R.; Luski, S.; Brousse, T.; Aurbach, D. Carbon-based compsite materials for supercapacitor electrodes: a review. *J. Mater. Chem. C. A.* **2017**, *5* (5), 12653−12672.

(15) Jiang, H.; Lee, P. S.; Li, C. 3D carbon based nanostructures for advanced supercapators. *Energy Environ. Sci.* **2013**, *6*, 41−53.

(16) Kazemi, S. H.; Kiani, M. A.; Ghaemmaghami, M.; Kazemi, H. Nano-architectured MnO$_2$ electrodeposited on the Cu-decorated nickel foam substrate as supercapacitor electro- de with excellent areal capacitance. *Electrochim. Acta* **2016**, *197*, 107−116.

(17) Asen, P.; Shahrokhian, S. A high performance supercapacitor based on graphene/- pollypyrrole/Cu$_2$O-Cu(OH)$_2$ ternary nano-composite coated on nickel foam. *J. Phys. Chem. C.* **2017**, *121*, 6508−6519.

(18) Ansari, M. Z.; Parveen, N.; Nandi, D. K.; Ramesh, R.; Ansari, S. A.; Cheon, T.; Kim, S. H. Enhanced activity of highly conformal and layered tin sulfide (SnSx) prepared by atomic layer deposition (ALD) on 3D metal scaffold towards high performance supercapacitor electrode. *Sci. Rep.* **2019**, *9*, 10225.

(19) Cherusseri, J.; Choudhary, N.; Kumar, K. S.; Jung, Y.; Thomas, J. Recent trends in transition metal dichalcogenide based super-capacitor electrodes. *Nanoscale Horiz.* **2019**, *4*, 840−858.

(20) Bissett, M. A.; Worrall, S. D.; Kinloch, I. A.; Dryfe, R. A. Comparison of two- dimensi- nal transition metal dichalcogenides for electrochemicalsupercapacitors. *Electrochim. Acta* **2016**, *201*, 30−37.

(21) Xu, W.; Xie, Z.; Cui, X.; Zhao, K.; Zhang, L.; Dietrich, G.; Dooley, K. M.; Wang, Y. Hierachiical graphene-encapsulated hollow SnO$_2$@SnS$_2$ nanostructures with enhanced lithium storage capability. *ACS Appl. Mater. Interfaces* **2015**, *7*, 22533−22541.

(22) Joseph, A.; Anjitha, C. R.; Aravind, A.; Aneesh, P. M. Structural, optical and magnetic properties of SnS$_2$ nanoparticles and photo response characteristics of p-Si/n-SnS$_2$ heterojunction diode. *Appl. Surf. Sci.* **2020**, *528*, 146977.

(23) Jing, L.; Xu, Y.; Chen, Z.; He, M.; Xie, M.; Liu, J.; Xu, H.; Huang, S.; Li, H. Different morphologies of SnS$_2$ supported on 2Dg-C$_3$N$_4$ for excellent and stable visible light photocatalytic hydrogen generation. *ACS Sustainable Chem. Eng.* **2018**, *6*, 5132−5141.

(24) Zhao, J.; Konh, M.; Teplyakov, A. Surface Chemistry of Thermal Dry Etching of Cobalt Thin Films Using Hexafluoroacety-lacetone (hfacH). *Appl. Surf. Sci.* **2018**, *455*, 438−445.

(25) Cui, X.; Xu, W.; Xie, Z.; Wang, Y. High-performance dye-sensitized solar cells based on Ag-doped SnS_2 counter electrodes. *J. Mater. Chem. A* **2016**, *4*, 1908−1914.

(26) Wan, Q.; Chen, X.; Gui, Y. First-principles insight into a Ru-doped SnS_2 monolayer as a promising biosensor for exhale gas analysis. *ACS Omega* **2020**, *5*, 8919−8926.

(27) Deng, L.; Zhu, J.; Chen, X.; Ding, M.; Liu, H. Three-dimensional elastic ultrathin redu- ced graphene oxide coating SnS_2 hierarchical microsphere as lithium ion batteries anode materials. *J. Alloys Compd.* **2018**, *739*, 1015−1024.

(28) Jiang, Y.; Wei, M.; Feng, J.; Ma, Y.; Xiong, S. Enhancing the cycling stability of Na- ion batteries by bonding SnS_2 ultrafine nanocrystals on amino-functionalized graphene hy- brid nanosheets. *Energy Environ. Sci.* **2016**, *9*, 1430−1438.

(29) Enaganti, P. K.; Selamneni, V.; Sahatiya, P.; Goel, S. MoS_2/cellulose paper coupled with SnS_2 quantum dots as 2D/0D electrode for high-performance flexible supercapacitor. *New J. Chem.* **2021**, *45*, 8516−8526.

(30) Li, B.; Xing, T.; Zhong, M.; Huang, L.; Lei, N.; Zhang, J.; Li, J.; Wei, Z. A two-dimensional Fe-doped SnS_2 magnetic semiconductor. *Nat. Commun.* **2017**, *8* (1), 1958.

(31) Shown, I.; Samireddi, S.; Chang, Y. C.; Putikam, R.; Chang, P. H.; Sabbah, A.; Fu, F. Y.; Chen, W. F.; Wu, C. I.; Yu, T. Y.; Chung, P. W. Carbon-doped SnS_2 nanostructure as a high-efficiency solar fuel catalyst under visible light. *Nat. Commun.* **2018**, *9*, 169.

(32) Fu, S.; Ma, L.; Gan, M.; Shen, J.; Li, T.; Zhang, X.; Zhan, W.; Xie, F.; Yang, J. Sn-doped nickel sulfide (Ni_3S_2) derived from bimetallic MOF with ultra high capacitance. *J. Alloys Compd.* **2021**, *859*, 157798.

(33) Afzali, N.; Beydokhti, M. T.; Khodadadi, A. A.; Mortazavi, Y. Tuning the band-gap and enhancing the trichloroethylene photo-catalytic degradation activities of flower-like Ni-doped SnS_2/SnO_2 heterostructures by partial oxidation. *J. Environ. Chem. Eng.* **2022**, *10*, 107793.

(34) Chen, D.; Huang, S.; Huang, R.; Zhang, Q.; Le, T. T.; Cheng, E.; Yue, R.; Hu, Z.; Chen, Z. Construction of Ni-doped SnO_2-SnS_2 heterojunctions with synergistic effect for enhanc-ed photodegrada-tion activity. *J. Hazard. Mater.* **2019**, *368*, 204−213.

(35) Wang, L.; Zhao, Q.; Wang, Z.; Wu, Y.; Ma, X.; Zhu, Y.; Cao, C. Cobalt-doping SnS_2 nanosheets towards high-performance anodes for sodium ion batteries. *Nanoscale* **2020**, *12*, 248−255.

(36) Setayeshmehr, M.; Haghighi, M.; Mirabbaszadeh, K. Binder-free 3D flower-like alkali doped-SnS_2 electrodes for high-performance supercapacitors. *Electrochim. Acta* **2021**, *376*, 13s7987.

(37) Parveen, N.; Ansari, S. A.; Alamri, H. R.; Ansari, M. O.; Khan, Z.; Cho, M. H. Facile sy- nthesis of SnS_2 nanostructures with different morphologies for high-performance supercar- pacitor applications. *ACS Omega* **2018**, *3*, 1581−1588.

(38) Wang, L.; Ma, Y.; Yang, M.; Qi, Y. One-pot synthesis of 3D flower-like hetrostrucured SnS_2/MoS_2 for enhanced supercapacitor behavior. *RSC Adv.* **2015**, *5*, 89069−89075.

(39) Mishra, R. K.; Baek, G. W.; Kim, K.; Kwon, H. I.; Jin, S. H. One-step solvothermal synt- thesis of carnation flower-like SnS_2 as superior electrodes for supercapacitor applications. *Appl. Surf. Sci.* **2017**, *425*, 923−931.

(40) Ansari, S. A.; Cho, M. H. Growth of three-dimensional flower-like SnS_2 on gC_3N_4 shee- ts as an efficient visible-light photocatalyst, photoelectrode, and electrochemical supercap- acitance material. *Sustainable Energy Fuels* **2017**, *1*, 510−519.

(41) Ma, L.; Xu, L.; Zhou, X.; Xu, X.; Zhang, L. Molybdenum-doped few-layered SnS_2 ar- chitectures with enhanced electrochemical supercapacitive performance. *RSC Adv.* **2015**, *5* (128), 105862−105868.

(42) Asen, P.; Haghighi, M.; Shahrokhian, S.; Taghavinia, N. One step synthesis of SnS_2-SnO_2 nano-heterostructured as an electrode material for supercapacitor applications. *J. Alloys Compd.* **2019**, *782*, 38−50.

(43) Chauhan, H.; Singh, M. K.; Kumar, P.; Hashmi, S. A.; Deka, S. Development of SnS_2/R GO nanosheet composite for cost-effective aqueous hybrid supercapacitors. *Nanotechnolgy* **2017**, *28* (2), 025401.

(44) Sajjad, M.; Khan, Y.; Lu, W. One-pot synthesis of 2D SnS_2 nanorods with high energy density and long term stability for high-performance hybrid supercapacitor. *J. Energy Storage* **2021**, *35*, 102336.

(45) Meng, X.; Zhou, M.; Li, X.; Yao, J.; Liu, F.; He, H.; Xiao, P.; Zhang, Y. Synthesis of - SnO_2 nanoflowers and electrochemical properties of Ni/SnO_2 nanoflowers in supercapacit- or. *Electrochim. Acta* **2013**, *109*, 20−26.

(46) Chu, H.; Zhang, F.; Pei, L.; Cui, Z.; Shen, J.; Ye, M. Ni, Co and Mn doped SnS_2-graphene aerogels for supercapacitors. *J. Alloys Compd.* **2018**, *767*, 583−591.

(47) Yin, J.; Zheng, C.; Qi, L.; Wang, H. Concentrated $NaClO_4$ aqueous solutions as promi- sing electrolytes for electric double-layer capacitors. *J. Power Sources* **2011**, *196*, 4080−4087.

(48) Wang, J.; Huang, J.; Huang, S.; Notohara, H.; Urita, K.; Moriguchi, I.; Wei, M. Ration- al design of hierarchical SnS_2 microspheres with S vacancy for enhanced sodium storage perform-ance. *ACS Sustainable Chem. Eng.* **2020**, *8*, 9519−9525.

(49) Ren, Y.; Lv, W.; Wen, F.; Xiang, J.; Liu, Z. Microwave synthesis of SnS_2 nanoflakes anchored graphene foam for flexible lithium-ion battery anodes with long cycling life. *Mater. Lett.* **2016**, *174*, 24−27.

(50) Ma, D.; Zhou, H.; Zhang, J.; Qian, Y. Controlled synthesis and possible formation me- chanism of leaf-shaped SnS_2 nanocrystals. *Mater. Chem. Phys.* **2008**, *111*, 391−395.

(51) Liu, K.; Wang, J. A.; Lou, C.; Zhou, Z.; Zhang, N.; Yu, Y.; Zhang, Q.; Henkelman, G.; Tang, M.; Sun, J. Simple construction and reversible sequential evolution mechanism of nitrogen-doped mesoporous carbon/SnS2 nanosheets in lithium-ion batteries. *Appl. Surf. Sci.* **2023**, *618*, 156673.

(52) Li, L.; Gao, J.; Cecen, V.; Fan, J.; Shi, P.; Xu, Q.; Min, Y. Hierarchical WS2@ $NiCo_2$- O_4 core−shell heterostructure arrays supported on carbon cloth as high-performance electr- odes for symmetric flexible supercapacitors. *ACS Omega* **2020**, *5*, 4657−4667.

(53) Dong, J.; Hou, Z.; Zhao, Q.; Yang, Q. Synthesis and characterization of nickel-doped manganese dioxide electrode materials for supercapacitors. *E3S Web Conf.* **2019**, *79*, 03002.